Gas temperature measurements from ps-TALIF in highly collisional plasmas

Abdoulaye Constant Siby, Dimitrios Stefas, Yanis Agha, Laurent Invernizzi, Kristaq Gazeli, Guillaume Lombardi, Khaled Hassouni, Swaminathan Prasanna

Usefulness of ps-TALIF for gas temperature measurements in a highly collisional Hydrogen plasma

Abdoulaye Siby, Dimitrios Stefas, Yanis Agha, Laurent Invernizzi, Kristaq Gazeli, Guillaume Lombardi, Khaled Hassouni, and Swaminathan Prasanna*

Laboratoire des Sciences des Procédés et des Matériaux (LSPM)

CNRS, UPR 3407, Université Sorbonne Paris Nord,

99 avenue J.B. Clément, 93430 Villetaneuse, France

(Dated: August 23, 2023)

Abstract

In this work, we present and discuss simultaneous measurements of H-atom absolute densities and gas temperatures performed in a moderate-pressure microplasma of pure hydrogen using an advanced ps-TALIF diagnostic. Furthermore, the use of a streak camera allows for the measurement of the effective lifetime of the laser excited species τ_H of ps-time scales. It has been shown that the retrieval of gas temperatures from τ_H is possible provided the collisionality criterion $\gamma \rightarrow 1$. Thus, this methodology was applied to obtain a 2D distribution of gas temperature and H-atom densities in the downstream region of the microplasma discharge.

* swaminathan.prasanna@lspm.cnrs.fr

Optical diagnostics of collisional plasmas allow for a basic understanding of the local reactive conditions by serving as useful indicators that reveal complex processes taking place in reactive flows. The fundamental philosophy of these diagnostics is to probe a radiative chemical species[1, 2]. Gas temperature (T_g) is one of the most important fundamental property whose accurate measure- ment is still complicated in a strongly non-equilibrium reactive plasmas. Different non-invasive optical methods such as rotational emission spectra [3], light scattering techniques [4], Coherent anti-Stokes Raman spectroscopy (CARS) [5] etc. have been proposed for its measurement while the development of new techniques continues to attract active interest. In this paper we use picosecond (ps) Two Photon Absorption Laser Induced Fluorescence (TALIF) to directly measure the effective lifetime of H(n=3) laser excited state in a highly collisional H_2 plasma, and deduce T_g from the determined effective lifetime.

TALIF has become the standard approach to measure atom densities in reactive environments [6]. The principle of TALIF is to excite the ground-state atoms by absorption of two photons of a pulsed laser to a fluorescing state and subsequently recording the resulting fluorescence signal. TALIF can also be used to probe non-emissive region of the discharge unlike the methods such as actinometry that are based on measuring intensities of plasma induced emissive lines of atoms. Moreover, compared to other known optical methods such as absorption spectroscopy and actinometry, TALIF measurements achieves better spatial resolution with temporal resolution as low as ps timescales[6].

However, performing TALIF diagnostics in highly collisional environments remains challenging. For most collisional reactive conditions encountered in a moderate- to high-pressure discharges, the effective lifetime is of sub-nanosecond or ps time scale, thus using ps lasers become necessary. Moreover, owing to the sensitivity of the atom density measurements to the effective lifetime of the laser excited species τ_X, it also becomes necessary to use an acquisition system with a time resolution sufficient to capture the decay process. In the absence of an ultrafast acquisition system, one has to use approximate models to estimate the effective lifetimes that are absolutely necessary for measuring of atom densities. More often, such models approximate the local conditions such as temperature, molar fractions of quenchers and pressure which limits the accuracy of the estimated atom densities.

Moreover, the effective lifetime measured from TALIF signals serves as a probe to the different collisional-radiative processes associated with the local plasma conditions and there-

fore can be used to probe the gas temperature. To demonstrate this, we have used a MW microplasma source operating with pure hydrogen under moderate pressure conditions ranging between 50 to 125 mbar. The experimental setup used for the present study is depicted in Figure 1 showing the optical diagnostic system, ps-laser, streak camera and the reactor chamber housing the MW plasma source.

Detailed description of ps-laserand streak camera have been provided in [7, 8]. In brief, the ps-laser system can generate pulses with a width of 10 ps at a repetition frequency of 5 Hz in the spectral range 193-2300 nm. A laser pulse up to 60 μJ/pulse can be generated at the two-photon excitation wavelength of H at 205.03 nm. A fused-silica lens with a focal length 500 mm was used to obtain a laser spot size with diameter of 500 μ m at the center of the plasma chamber. The laser beam exiting the plasma chamber is collected by means of a calorimeter connected to a digital oscilloscope to measure the energy of the laser. The energy of the laser was controlled using the internal amplification of the laser system and a combination of neutral density filters. The fluorescence signal was collected perpendicular to the laser beam using a achromatic lens of 100 mm focal length and a band-pass filter mounted in front of the entrance slit of the streak camera. Optical emission spectrocopy (OES) has been performed independently using a spectrometer having focal length of 1m (THR1000) to validate the results of ps-TALIF.

An in-house developed MW plasma microtorch based on coaxial transmission line resonator (CLTR) was used for the present work[9]. This torch has been used to produce carbon nanostructures such as nanodiamonds from gases H_2/CH_4 and Ar at moderate pressure ranges (20 to 150 mbar). The scope of this study is restricted to pure hydrogen plasmas. The plasma is generated in the small gap of 500 μm between the central metallic core and the coaxial ground. The microplasma torch was embedded into an octagonal vacuum chamber with three optical view-ports dedicated for laser diagnostics. The UV-laser beam passes through the chamber through the two fused-silica windows and the resulting fluorescence was collected perpendicularly through a borosilicate window. The flow rate of H_2 gas was set at 100 sccm for all the experiments, while the pressure in the chamber was maintained at the designated value using a pressure regulator. The reactor chamber was placed on a translation stage that allowed for moving the plasma along z with respect to the laser. The path of the laser was aligned with the x axis of the reactor with focus close to the axis of the microplasma.

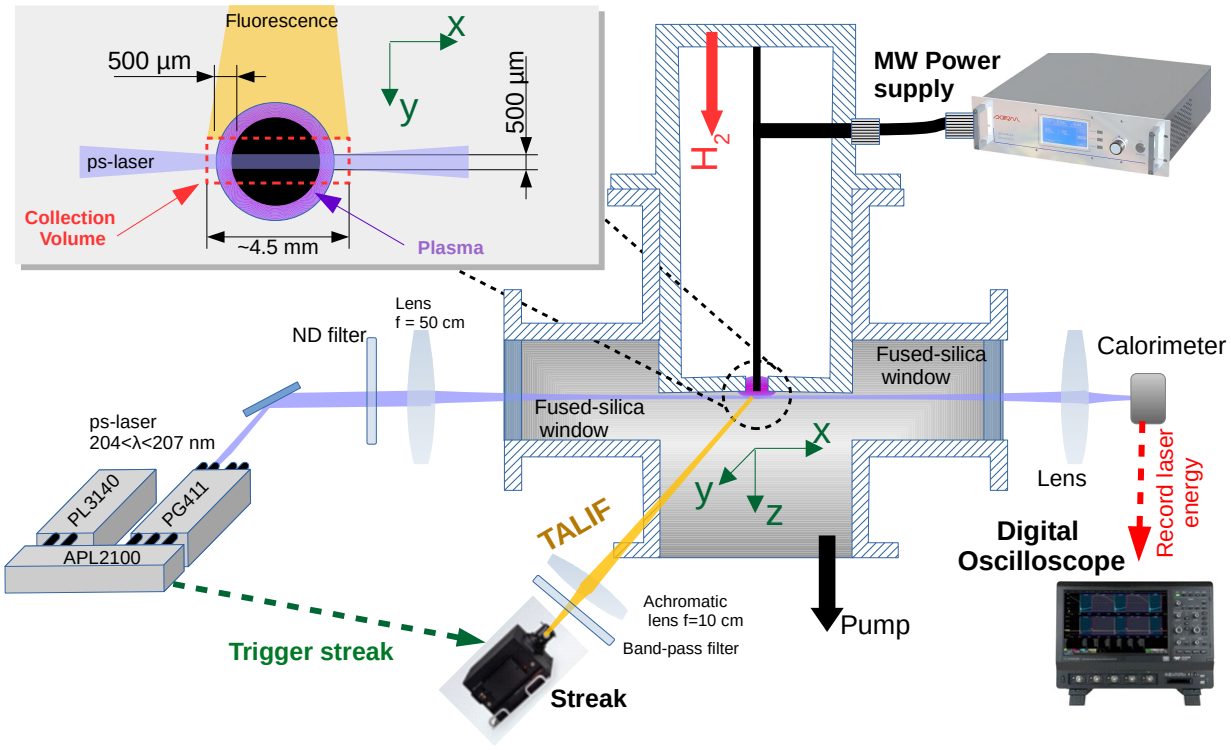

FIG. 1. Schematic of the experimental setup showing the layout of MW plasma reactor, ps-laser and streak camera.

The general principle of TALIF is discussed in [6]. The absolute density of atomic species i measured using TALIF can be written as

$$n_i = n_C \frac{\int_t \int_\lambda S_{F_i}}{\int_t \int_\lambda S_{F_C}} \frac{\eta_C}{\eta_i} \frac{T_C}{T_i} \frac{\sigma_C}{\sigma_i} \frac{A_C}{A_i} \frac{\tau_C}{\tau_i} \frac{E_C^2}{E_i^2} \frac{\lambda_C^2}{\lambda_i^2} \tag{1}$$

with subscript i and C referring to the reactive and calibrating atomic species respectively, n_i is the density of the reactive species i, $\int_t \int_\lambda S_{F_i}$ is the temporally and spectrally integrated fluorescence signal, η_i/η_C and T_i/T_C are the quantum efficiency of the detector and transmission of the optics at the fluorescence wavelength respectively, σ_i/σ_C is the two-photon excitation cross-section, A_i/A_C is the Einstein coefficient of the radiative decay of the laser excited state and τ_i/τ_C is the experimentally measured fluorescence decay time of the laser excited state, E_i/E_C and λ_i/λ_C are the energy and wavelength of the laser used for making the TALIF measurements. For performing ps-TALIF on H-atom, the H-atom ground-state is excited to the H(n=3) by absorption of two photons at an excitation wavelength of 205.08 nm and the resulting fluorescence is collected from the Balmer α line ($H_{n=3} \rightarrow H_{n=2}$) at 656.3 nm.

In equation 1, quantities $\int_t \int_\lambda S_{F_i}$ and τ_i are directly determined from ps-TALIF signals captured using a streak camera. Following Invernizzi et al. [8], the time window of the streak image was ideally set to 5 ns in order to accurately extract the τ_H over the range of experimental conditions. Actually, the raw TALIF signal captured using a streak camera is a 2D image where x-axis (673 pixels) and the y-axis (1016 pixels) are indicative of the spatial (i.e. x-axis of the reactor) and the temporal dimension respectively. The slit of the streak camera is horizontal and captures a zone of fluorescence of about 4.5 mm centered around the axis of the plasma torch as shown in Figure 1. However, accurate calibration between pixels and distance has not been done in this study. Nevertheless, moving point averaging was performed to suppress the noise in the raw images and obtain qualitatively the average spatial variation of the derived fields such as H-atom densities. The height of the plasma with respect to the laser (i.e. z) was changed in order to construct the 2D fields of H-atom density and other associated quantities in the x-z plane.

For making absolute density measurements, the H-atom density calibration was performed by replacing the plasma chamber by a quartz cuvette filled with Krypton at 200 Pa[10]. The quadratic dependence of the fluorescence intensity with respect to the a laser energy (as imposed by Equation 1) was verified for different operating conditions of H and Kr. However, as the optical parameters such as transmissivity, solid angle of cuvette and the plasma reactor are different, we determined their ratio from the ratio of H-atom densities obtained using ps-TALIF and actinometry. In actinometry, H-atom densities are estimated from the ratios of line intensities of H_α and Argon lines at 750.4 nm[11] of a H_2 plasma with $< 1\%$ of argon. This ratio was found to be 0.78 at a reference condition (pressure 100 mbar and 90 W power). This condition actually corresponds to the formation of diamond nanoparticles with a gas mixture of H_2-CH_4 [9]. This value was used for all subsequent measurements. Figure 2 compares the H-atom densities measured using ps-TALIF and actinometry. The good agreement between H-atom densities measured using ps-TALIF and actinometry for the other conditions gives us the confidence of our methodology.

τ_i characterizes the collisional and radiative decay processes of the excited species following the laser excitation and can be written as:

$$\frac{1}{\tau_i} = A_i + Q_i = A_i + \frac{P}{k_b T_g} \sum_{j}^{quenchants} k_{Q_{i/j}} x_j \tag{2}$$

Where Q_i and A_i are the quenching rate and the total Einstein coefficient of radiative decay

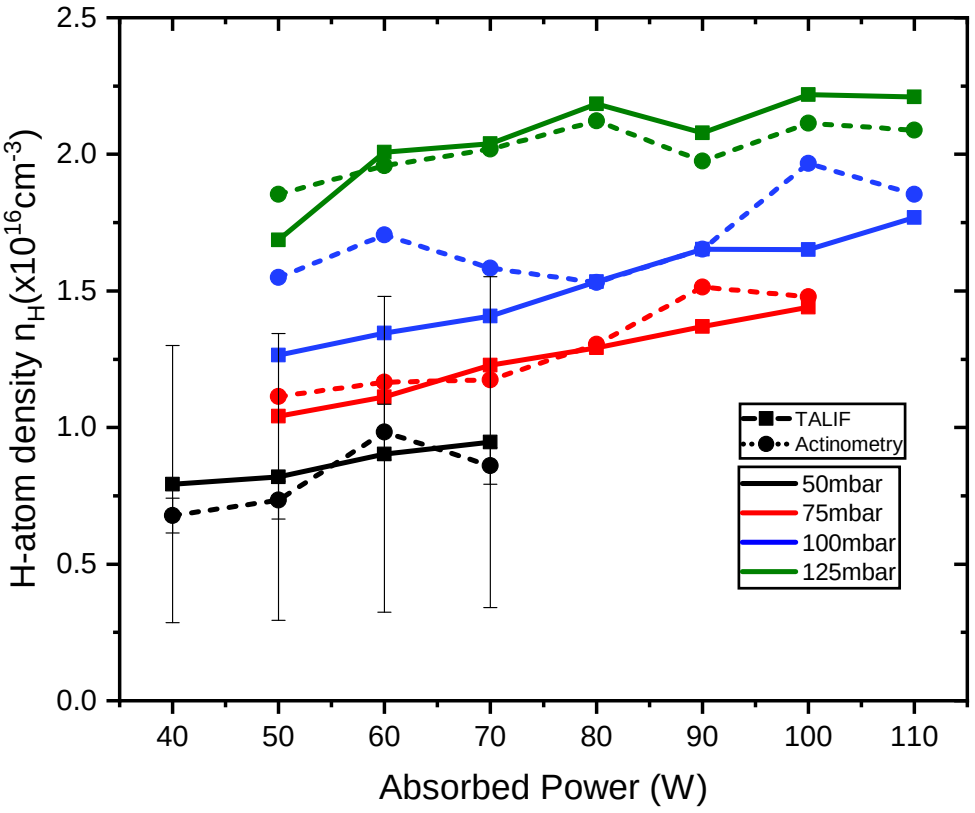

FIG. 2. Comparison of H-atom densities measured using actinometry and ps-TALIF as a function of pressure and power. The reference condition used for normalizing the ps-TALIF and actinometry has been chosen as 100 mbar Pressure and 90 W Power

of the excited state. P is the local pressure, T_g is the gas temperature, k_B is the Boltzmann constant, and x_j is the molar fraction of the quenchant j. $k_{Q_{i/j}}$ is the rate coefficient of quenching of excited species i by quenchant j and can be expressed as :

$$k_{Q_{i/j}} = \sigma_{Q_{i/j}} \nu_{i/j} = \sigma_{Q_{i/j}} \sqrt{\frac{8 k_B T_g}{\pi \mu_{i/j}}} \tag{3}$$

where $\sigma_{Q_{i/j}}$ is the collisional quenching cross section, $\nu_{i/j}$ and $\mu_{i/j}$ are the mean thermal velocity and the reduced mass of collision pair i/j.

The measurement of τ_i and exploitation of equation 2 allows one to gain more insight about the reactive environment. For example, one can determine radiative decay rate $1/A_i$ and collisional quenching cross-section $\sigma_{Q_{i/j}}$ using the Stern-Volmer plot of $\frac{1}{\tau_i}$ over a range

of pressures covering three distinct regimes:

- Radiation dominated regime at extremely low pressures i.e. $A_i >> Q_i$
- Collision dominated regime at moderate to high pressures where $A_i << Q_i$
- Competition between radiative and collisional processes at intermediate pressures i.e. $A_i \sim Q_i$

Similarly, with the knowledge of radiative and collisional decay constants, it would be possible to deduce the gas temperature T_g by rewriting equation 2 as

$$T_g = \frac{8}{\pi k_B} \left(\frac{P\tau_i}{1 - \tau_i A_i} \sum_j \frac{x_j \sigma_{Q_{i/j}}}{\sqrt{\mu_{i/j}}} \right)^2 \tag{4}$$

However, it is necessary to check the conditions of validity for estimating T_g from τ_i using equation 4. For simplicity, we make an approximation that there is equilibrium in translational temperature i.e. T_g of all heavy species and the collisional quenching rates are not affected by the thermal non-equilibrium that may exist in the vibrational and rotational modes of the quenchant heavy species. The most important condition that needs to be accounted for is the collisionality of the plasma $\gamma_i = 1 - \tau_i A_i$ which occupies the denominator of equation 4. It is easy to notice that γ_i varies between 0 and 1 where the lower asymptotic limit $\gamma_i \to 0$ is indicative of radiation dominated decay process while the opposite $\gamma_i \to 1$ is indicative of collisional dominated regime. It is obvious that the retrieval of temperature is not applicable for radiative dominated decay regimes (mathematically as $\gamma_i \to 0$, $T_g \to \infty$) . Moreover, the uncertainty analysis indicates that the propagation of errors is minimum when $\gamma \to 1$. For example, the errors emerging from different components can be amplified up to two folds when $\gamma_i = 0.5$. The τ_H decreases with increase in pressure, indicating increase in collisionality. For the conditions examined in this paper, the plasma is highly collisional with τ_H ranging between 100 and 450 ps while $\gamma_H > 0.95$ (calculated using $A_{H(n=3)} = 4.41 \times 10^7$ s^{-1} for Balmer α line[12]) as shown in Figure 3. Therefore, in principle, we are in the right conditions that allow us to make simultaneous measurement of H-atom density as well as T_g using the same fluorescence signal.

However, determination of τ_H with good confidence is absolutely necessary for reliable retrieval of T_g. Invernizzi et al.[8] discuss the challenges of accurately extracting τ_i from raw ps-TALIF signals captured with a streak camera by taking into account the apparatus

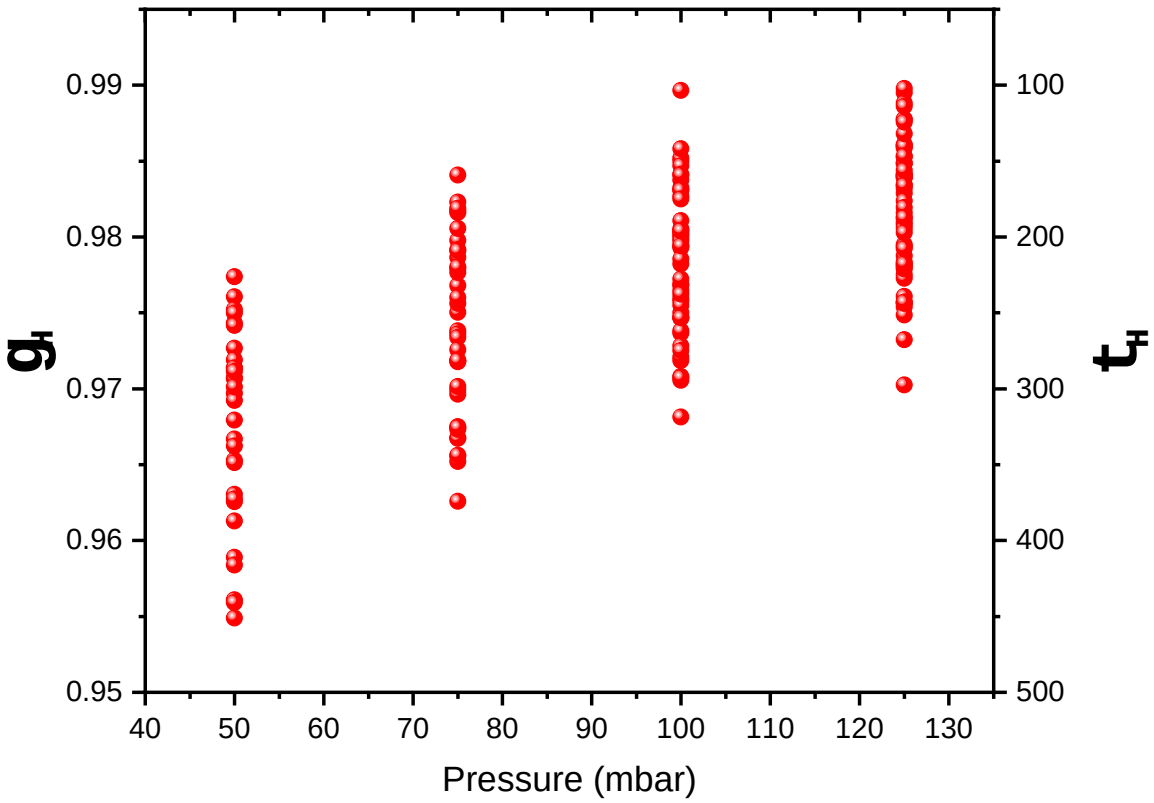

FIG. 3. Variation of τ_H extracted from ps-TALIF signals and corresponding γ_H as a function of pressure for the experimental conditions considered in this paper.

function of the detector, which must be deconvuluted from the raw ps-TALIF signal. The uncertainty of τ_i would naturally depend on the density of probing atomic species. Lower atom densities would indicate lower TALIF signal intensity as well as increased noise, which would make it difficult to accurately extract τ_i from the raw TALIF data, hence including a larger uncertainty. Uncertainty of τ_H was estimated within 5 % in our conditions to make the measurements of T_g reasonable.

The high-collisionality would mean that complex radiative processes that are associated to the $H(n = 3)$ level have little influence while the respective collisional processes dictate the values of τ_H. Therefore, as evident from equation 4, knowledge of all collisional quenchers and corresponding composition and cross-section is necessary. H_2 and H are the only quenchers for our conditions and their composition is already known from TALIF

measurements, albeit with huge uncertainty of n_H of 50%. Unfortunately, there exists huge uncertainty with regard to the σ_{H/H_2} of H_2 molecule with values ranging between 65 [13, 14] to 156 [15] A^2 reported in the literature. Recently, Corinne et al. discussed about the complex depopulation mechanisms of excited states of atomic hydrogen following ps two-photon excitation to the H(n=3) level and deduced σ_{H/H_2} to 98±10 A^2. On the other hand, H-atom is a weak quencher with a much smaller $\sigma_{H/H}$ of 3.8 A^2 [16] as compared to H_2.

Moving point average with a window size of 200 pixels (which covers approximately 1.5 mm) was applied to each streak image to construct the horizontal distribution of H-atom densities and corresponding retrieved T_g with different values of σ_{H/H_2}. The peak of gas temperatures obtained from τ_H and different values of σ_{H/H_2} have been compared with rotational temperature determined from the emission spectra of H_2 rotational bands of (i) R branch of the transition $G^1\sum_g^+$, $\nu' = 0 \rightarrow B^1\sum_u^+$, $\nu'' = 0$ and (ii) the Q-Branch $d^3\prod_u$, $\nu' = 0 \rightarrow a^3\sum_g^+$, $\nu''= 0$ of the Fulcher-α band [3, 17, 18] as shown in Figure 4(a). It has to be noted that rotational temperatures of G-band can be used as a good estimate for gas temperature for these pressure ranges [18]. However, the excited states of Fulcher do not equilibriate with the gas temperature at these pressure conditions[9, 19] and therefore the rotational temperature of Fulcher band would be lower than the gas temperature. Gas temperatures estimated using $\sigma_{H/H_2} = 65\ A^2$[13, 14] are far too low when compared to the rotational temperature of Fulcher to be realistic. Similarly, gas temperatures estimated using $\sigma_{H/H_2} = 156\ A^2$[15] are far too high to be realistic. However, the gas temperatures measured using $\sigma_{H/H_2} = 98\ A^2$ compares well (±25%) with those measured from emission spectra of G-band as shown in Figure 4(b). These results show that the σ_{H/H_2} proposed by Duluard et al. is reliable.

Analysis of propagation of errors indicates that the major contribution comes from the uncertainty of the collisional quenching cross-section σ_{H/H_2} for all the studied conditions. Due to low dissociation (< 5%) as well as weak quenching by H-atoms ($\sigma_{H/H} << \sigma_{H/H_2}$), H-atom density does not play a major role towards the temperature measurements. Therefore the only experimentally measured parameter that affects the temperature measurement is τ_H. Nevertheless, its contribution towards total uncertainty is low for most conditions with a maximum of 30% far away from the plasma zone where the temperature is much lower and close to ambient. However, due to the high uncertainty of σ_{H/H_2} of 10%, the minimum uncertainty of T_g translates to about 14% and marks the limitation of the present

methodology when compared with other laser based methods such as CARS and LIF that are based on measuring intensities of spectral lines.

However, since the present method allows for localised measurements to be performed, it also allows for the construction of axial temperature fields from a single fluorescence signal. 2D temperature fields were constructed by changing the laser beam position along z-axis in intervals of 1 mm. Figure 5 shows the 2D contour plot of H-atom density and gas temperature at different pressure conditions and are consistent with the characteristics of the discharge with pressure. Both H-atom and T_g are much more homogeneous axially at lower pressures such as 50 and 75 mbar. However, as the thermal diffusion decreases with higher pressures, one can clearly recognize two hot local zones separated by a cold zone close to $z = 0$ plane indicative of the annular shape of the microplasma. One can clearly observe that there is a strong dissociation of H-atoms locally in these hot zones at 125 mbar which are absent at lower pressures due to high diffusivity of H-atoms. This spatial variation of both H-atom and T_g could not be visually deciphered from the raw fluorescence signals and only the post-treatment of these signals allowed us to access the spatial characteristics. In fact, this made it difficult to accurately position the axis of the torch with respect to the center of the streak camera. More importantly, the method was able to capture the strong temperature gradients that are present in the present microplasma. The temperature differences between the hot-zones and surrounding regions were as high as 600 K. Also, there is a sharp decrease in temperature and H-atom density away from the plasma discharge and are homogeneous within 3 mm from the plasma region. T_g becomes closer to ambient temperature within about 5 mm from the discharge zone. However, there is still a substantial amount of H-atoms (1×10^{15} cm^{-1}) at such low temperatures which may be interesting for different applications such as elaboration of carbon nanostructures such as nandiamonds.

This work clearly demonstrates the reliable determination of temperatures from τ_H for highly collisional conditions. The major constraints that need to be satisfied for the gas temperature retrieval from τ_H using ps-TALIF are the following (i) a substantial concentration of H-atoms is needed to detect fluorescence, (ii) plasma collisionality must be $\gamma >> 0$ and (iii) collisional cross-sections of the different quenchers must be known. The extension of the present methodology to complex gas mixtures may be possible with careful considerations of different possible quenchers. Nevertheless, the philosophy discussed in this paper can

always be exploited to gather insight into the local conditions prevailing in a complex reactive flow. The merit of this method lies in the fact that both atom-densities as well as gas temperatures can be obtained simultaneously from a single fluorescence signal. Moreover, as the measurements are spatially local, 2D (or even 3D) cartography of gas temperature can be constructed.

ACKNOWLEDGEMENTS

This work was funded by the French Agence Nationale de la Recherche (ANR), under grants ANR-22-CE51-0013 (project NANODIAPLAS) and ANR-22-CE51-0027-02 (project ULTRAMAP) and IDF regional project SESAME DIAGPLAS. One of the authors (Khaled Hassouni) acknowledges the support of the Institut Universitaire de France.

---

[1] R. A. Gottscho and T. A. Miller, Pure and Applied Chemistry **56**, 189 (1984).

[2] R. Engeln, B. Klarenaar, and O. Guaitella, Plasma Sources Science and Technology **29**, 063001 (2020).

[3] P. J. Bruggeman, N. Sadeghi, D. C. Schram, and V. Linss, Plasma Sources Science and Technology **23**, 023001 (2014).

[4] N. M. Laurendeau, Progress in Energy and Combustion Science **14**, 147 (1988).

[5] S. Roy, J. R. Gord, and A. K. Patnaik, Progress in Energy and Combustion Science **36**, 280 (2010).

[6] K. Gazeli, G. Lombardi, X. Aubert, C. Y. Duluard, S. Prasanna, and K. Hassouni, plasma **4**, 145 (2021).

[7] K. Gazeli, X. Aubert, S. Prasanna, C. Duluard, G. Lombardi, and K. Hassouni, Physics of Plasmas **28**, 043301 (2021).

[8] L. Invernizzi, C. Y. Duluard, H. Höft, K. Hassouni, G. Lombardi, K. Gazeli, and S. Prasanna, Measurement Science and Technology **34**, 095203 (2023).

[9] Z. Jia, Y. Fermi, A. Siby, O. Brinza, K. Hassouni, and S. Prasanna, Plasma Processes and Polymers **20**, 2200180 (2023).

[10] S. Schröter, J. Bredin, A. R. Gibson, A. West, J. P. Dedrick, E. Wagenaars, K. Niemi, T. Gans, and D. O'Connell, Plasma Sources Science and Technology **29**, 105001 (2020).

[11] A. Gicquel, M. Chenevier, K. Hassouni, A. Tserepi, and M. Dubus, Journal of applied physics **83**, 7504 (1998).

[12] W. Wiese and J. Fuhr, Journal of physical and chemical reference data **38**, 565 (2009).

[13] U. Meler, K. Kohse-Höinghaus, and T. Just, Chemical physics letters **126**, 567 (1986).

[14] J. Bittner, K. Kohse-Höinghaus, U. Meier, and T. Just, Chemical Physics Letters **143**, 571 (1988).

[15] A. Catherinot, B. Dubreuil, and M. Gand, Physical Review A **18**, 1097 (1978).

[16] F. Brouillard and X. Urbain, Physica Scripta **2002**, 86 (2002).

[17] M. M. Vasiljević, G. L. Majstorović, D. Spasojević, and N. Konjević, European Physical Journal D **75**, 112 (2021), aDS Bibcode: 2021EPJD...75..112V.

[18] A. Gicquel, K. Hassouni, Y. Breton, M. Chenevier, and J. C. Cubertafon, Diamond and Related Materials **5**, 366 (1996).

[19] R. Garg, T. Anderson, R. Lucht, T. Fisher, and J. Gore, J. Phys. D: Appl. Phys. **41**, 095206 (2008).

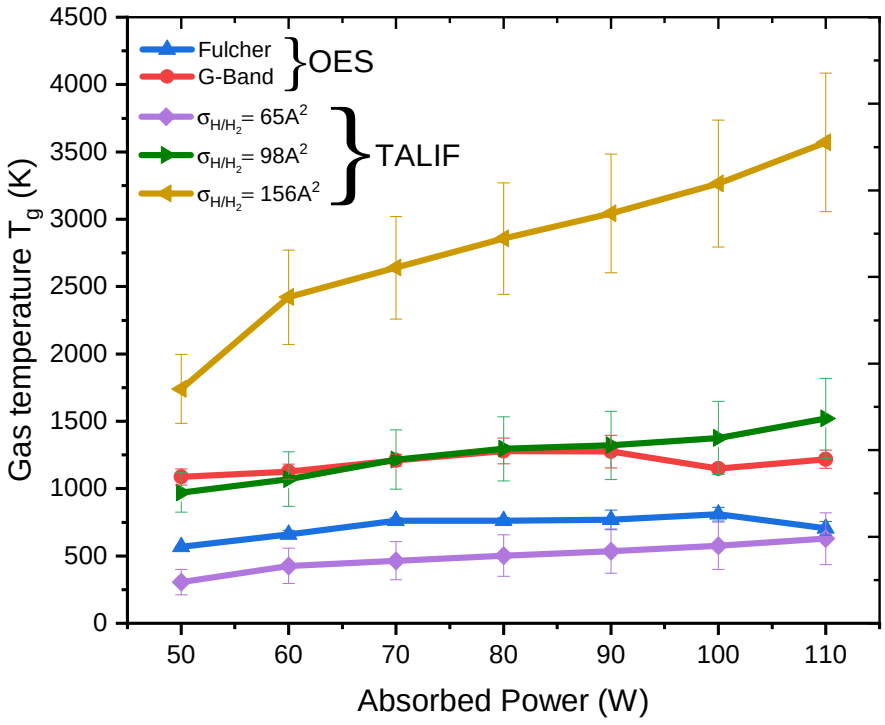

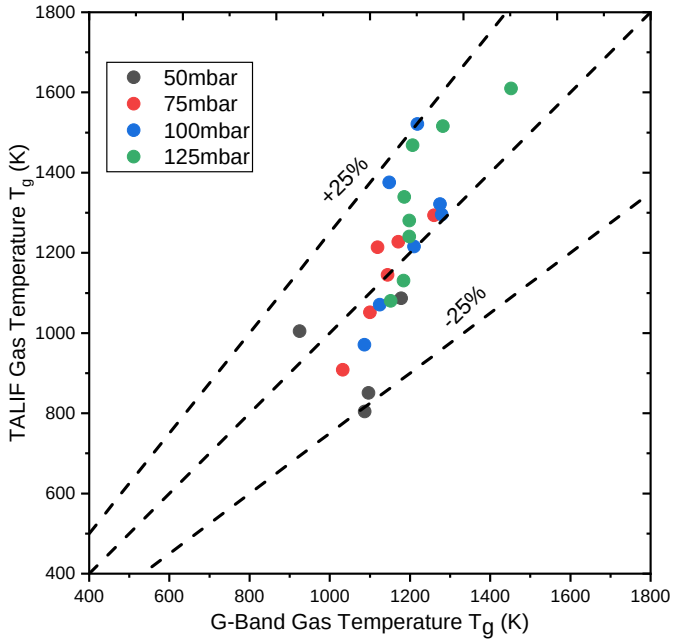

FIG. 4. (a) Comparison of gas temepratures measured using OES and ps-TALIF at 100 mbar and (b) parity plot comparing gas temperature measurement using G-band and ps-TALIF using $\sigma_{H/H_2} = 98\ A^2$.

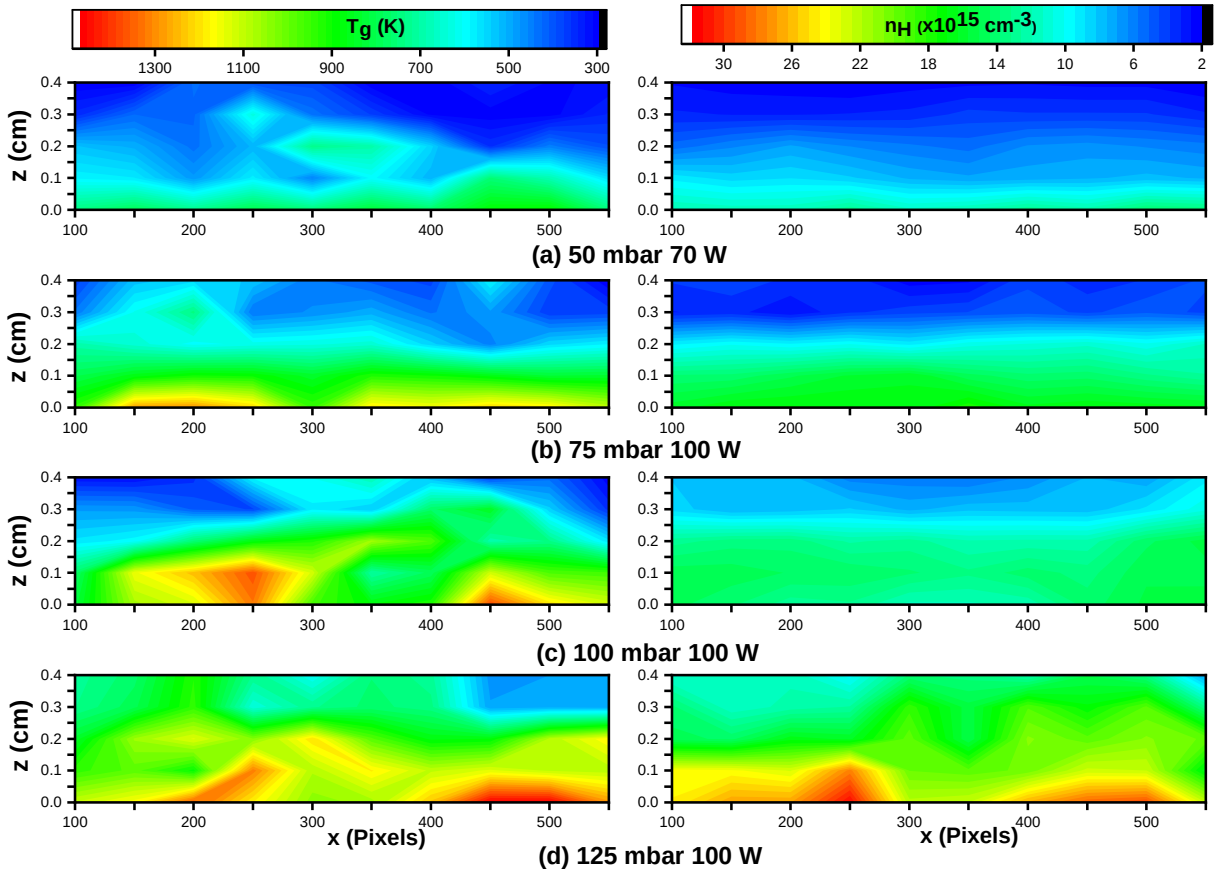

FIG. 5. Constructed 2D contour plots of H-atom density and T_g for different pressures. The x-axis is referred to in pixels as axial calibration (i.e. along x-axis) was not performed. y-axis refers to z with 0 referring to the first possible laser measurement which is about 0.5 mm from the base of the torch.